CERN-PH-TH/2006-056,
IFJPAN-IV-2006-3

Next to Leading Logarithms and the PHOTOS Monte Carlo

P. Golonka and **Z. Wąs**
CERN, 1211 Geneva 23, Switzerland
and
Institute of Nuclear Physics, PAN, Kraków, ul. Radzikowskiego 152, Poland

ABSTRACT

With the approaching start-up of the experiments at LHC, the urgency to quantify systematic uncertainties of the generators, used in the interpretation of the data, is becoming pressing. The PHOTOS Monte Carlo program is often used for the simulation of experimental, selection-sensitive, QED radiative corrections in decays of Z bosons and other heavy resonances and particles. Thanks to its complete phase-space coverage it is possible, with no approximations for any decay channel, to implement the matrix-element. The present paper will be devoted to those parts of the next-to-leading order corrections for Z decays which are normally missing in PHOTOS. The analytical form of the exact and truncated, *standard*, kernel used in PHOTOS will be explicitly given. The correction, being the ratio of the exact to the approximate kernel, can be activated as an optional contribution to the internal weight of PHOTOS.

To calculate the weight, the information on the effective Born-level Z/γ^* couplings and even directions of the incoming beams, is needed. A universal implementation would have made the PHOTOS solution less modular and less convenient for the users. That is why, for the time being, we will keep the correcting weight as an extra option, available for special tests only.

We will quantify the numerical effect of the approximation with the help of a multitude of distributions. The numerical size of the effect is in general below 0.1%; however, in some corners of the phase-space (well defined and contributing less than 0.5% to the total rate), it may reach up to about 20% of their relative size.

CERN-PH-TH/2006-056,
IFJPAN-IV-2006-3
April, 2006

Supported in part by the EU grant MTKD-CT-2004-510126, in partnership with the CERN Physics Department, and the Polish State Committee for Scientific Research (KBN) grant 2 P03B 091 27 for years 2004–2006.

1. Introduction

Analysing the data from high-energy physics experiments, we try to solve the *"experiment = theory"* equation. This non-trivial task requires many different effects to be considered simultaneously. From the experimental side, these are mainly detector acceptance and cuts, which are dictated by the construction and physical properties of the detector: the shapes of distributions may be distorted by, say, misidentification and residual background contamination; these effects need to be discriminated in an appropriate and well-controlled way. From the theoretical side, *all* effects of known physics have to be included in predictions as well. Only then can experimental data and theoretical predictions be confronted to determine numerical values of some coupling constants or effects of new physics (to be discovered).

A well-defined class of theoretical effects contains the QED radiative corrections. PHOTOS is a universal Monte Carlo algorithm that simulates the effects of these corrections in decays of particles and resonances. It is a project with a rather long history: the first version was released in 1991 [1], followed by version 2.0 [2] (double emission, threshold terms for fermions). The package is in wide use [3]: it was applied as a precision simulation tool for W mass measurement at the Tevatron [4] and LEP [5, 6], and for CKM matrix measurements in decays of K and B resonances (NA48 [7], KTeV [8], Belle [9], BaBar [10] and at Fermilab [11]).

Throughout the years the core algorithm for the generation of $O(\alpha)$ corrections did not change much; however, its precision, applicability to various processes, and numerical stability improved significantly. New features, such as multiple photon radiation or interference effects for all possible decays, were also introduced.

Growing interest in the algorithm expressed by the experimental collaborations (including the future LHC experiments) was a motivation to perform a more detailed study of the potential and precision of the PHOTOS algorithm. The present paper is the third in the series [12, 13]. It is devoted to the Z boson decay and to simplifications in the matrix element used in PHOTOS for that channel. We also explore the limitations originating from compromises introduced into PHOTOS bremsstrahlung kernels, which assured convenience of use; no process-dependent weight need be involved.

In that respect, the study of the PHOTOS *matrix element* can be understood as a part of the on-going effort to find the practical solutions of the improved expansions. Some aspects of our solution resemble those of classical exclusive exponentiation as described in [14, 15]; in an other, the parton shower may be identified. The solution may be understood as a rearrangement of the QED perturbation expansion, yet this point will not be discussed here. Instead, let us point to some similarities of the PHOTOS solution to the methods discussed elsewhere: interaction picture of Quantum Mechanics, expansion of special functions around asymptotic solutions [16] or in field theory; see eg. [17]. In PHOTOS the expansion is performed in terms of multidimensional operators.

The paper is organized as follows. In Section 2 the main properties used in the PHOTOS design and, in particular, the analytical form of the (NLO) weight, necessary to introduce the complete first-order matrix-element, are presented. It is also explained there how the complete matrix elements break the requirement of separation of the calculation of the final-state

bremsstrahlung from the properties of the Born-level matrix elements and the phenomena affecting the Z production. To support the discussion and visualize the results, a multitude of numerical comparisons and tests will be presented. Section 3 provides the definition of the method used in those comparisons. The method is particularly suitable to visualize the results in the non-collinear regions of the phase space. Section 4 presents numerical tests performed at fixed first order of the QED expansion. Since PHOTOS uses the same building block for a part of the single-photon generation algorithm and for the multiple bremsstrahlung, the results presented in this section have implications for the multiple-photon option of PHOTOS. Section 5 addresses these aspects of the program construction which are relevant to the use of the NLO weight in the multiple-photon option. Section 6 collects the results of the tests performed for the programs run with multiple-photon emission. Summary, Section 7, closes the paper.

2. Phase space and matrix element

To discuss the implementation of the complete first-order QED radiative corrections in Z decay, we must start with the complete parametrization of the phase space.

Let us start with the explicit expression for the parametrisation of the $(n+1)$-body final state in the decay of an object of four-momentum P. To define iterative relations, let us denote the four-momenta of the first n decay products as k_i, and the last $(n+1)$-th as q. For the case discussed here, the $(n+1)$-th particle will always be the real and massless photon. However, the parametrization does not rely on this assumption and, in principle, can be applied to define other formulas for the phase space, such as the emission of a (massive) pion, and could even be extended to the case of emission of pairs of heavy particles. In later steps of our construction the fact that photons are massless and the related properties of QED matrix elements will of course be used.

In the following, the notations from refs. [18,19] will be used. We will, however, not rely on any particular results of those papers and only point to the more detailed presentations of other, nonetheless quite similar, options for the exact n-body phase-space parametrization to the one presented here.

Let us define the element of Lorentz-invariant phasespace (*Lips*) as follows:

$$\begin{aligned}
& dLips_{n+1}(P) = \\
& \frac{d^3k_1}{2k_1^0(2\pi)^3}\cdots\frac{d^3k_n}{2k_n^0(2\pi)^3}\frac{d^3q}{2q^0(2\pi)^3}(2\pi)^4\delta^4\Big(P-\sum_1^n k_i - q\Big) \\
= \;& d^4p\delta^4(P-p-q)\frac{d^3q}{2q^0(2\pi)^3}\frac{d^3k_1}{2k_1^0(2\pi)^3}\cdots\frac{d^3k_n}{2k_n^0(2\pi)^3}(2\pi)^4\delta^4\Big(p-\sum_1^n k_i\Big) \\
= \;& d^4p\delta^4(P-p-q)\frac{d^3q}{2q^0(2\pi)^3}dLips_n(p\to k_1\ldots k_n). \qquad (1)
\end{aligned}$$

Extra integration variables, the four-vector p, compensated with $\delta^4\left(p-\sum_1^n k_i\right)$, are first introduced. In the next step, another integration variable M_1 and $\delta\left(p^2-M_1^2\right)$ are introduced. The element of the phase-space integration may thus be transformed into:

$$\begin{aligned} & dLips_{n+1}(P) = \\ & \frac{dM_1^2}{(2\pi)} dLips_2(P \to p\ q) \times dLips_n(p \to k_1 \ldots k_n) \\ = \quad & dM_1^2 \left[d\cos\theta d\phi \frac{1}{8(2\pi)^3} \frac{\lambda^{\frac{1}{2}}(M^2, M_1^2, m^2)}{M^2} \right] \times dLips_n(p \to k_1 \ldots k_n). \end{aligned} \tag{2}$$

The part of the phase-space Jacobian corresponding to the integration over the direction and the energy of the last particle (or invariant mass of the remaining system) is explicitly given; $\lambda(a,b,c) = a^2+b^2+c^2-2ab-2ac-2bc$. The integration over the angles is defined in the rest frame of $n+1$ particles; the integration over the invariant mass M_1 is limited by the phase-space boundaries. There is no need to choose the axes with respect to which the angles are oriented; we will not elaborate on that point here, as details can be found in Ref. [1]. Formula (2) may be iterated to provide parametrization of the phase space with an arbitrary number of final-state particles. The question of the orientation of the reference frames used to define the angles and the order of the choice for limits in M_i integrations, becomes particularly complex then; our choice is described in ref. [2]. Since nothing new was introduced for the purpose of the present study we will not discuss this interesting point further. Except for the details mentioned above, the choice we made for the phase-space organization is the same as in FOWL [20], TAUOLA [19], and probably many other generators.

To simplify the formula for the phase space, let us finally take advantage of the zero mass of the photon. The invariant mass of the system of all particles but the first one may be replaced by the energy of the first one (defined in the P rest frame). The phase-space formula can then be written as:

$$\begin{aligned} & dLips_{n+1}(P) = \\ & \left[4dk_\gamma k_\gamma d\cos\theta d\phi \frac{1}{8(2\pi)^3} \right] \times dLips_n(p \to k_1 \ldots k_n) \\ = \quad & \left[k_\gamma dk_\gamma d\cos\theta d\phi \frac{1}{2(2\pi)^3} \right] \times dLips_n(p \to k_1 \ldots k_n). \end{aligned} \tag{3}$$

If we had l photons accompanying n other particles, the factor in square brackets would be iterated. A statistical factor $\frac{1}{l!}$ would complete the formula for the phase-space parametrization, which is quite similar to the formal expansion of the exponent[1]. The last formula, supplemented

[1]The exact form of the functional exponent is achieved if the four-vector p is replaced by P in formula (3). In this way the tangent space for the $(n+1)$-body phase space can be constructed. We use that space, together with an eikonal-like form of the matrix element (emissions from individual final-state charged products are treated as

with the definition of the orientation of the angles, is used to define the full kinematic configuration of the event. The four-momenta of all final-state particles may now be constructed from the angles and energies (k_{γ_i}) of the photons, and the angles and masses of the other decay products.

Similarly, an inverse operation may be performed; the energies and angles for the parametrization could be reconstructed from the four-vectors (even though the parametrization was not necessarily used in the previous generation steps). The phase-space Jacobians may be easily calculated as well. By replacing $dLips_n(p \to k_1 \ldots k_n)$ in formula (3) by $dLips_n(P \to k_1 \ldots k_n)$ we obtain a parametrization where the photons do not affect the construction of other particles' momenta. This operation could be considered as treating the photon in an approximation valid only in the soft photon limit. This, however, *does not need* to be the case. In the first step, the photon may be constructed with an arbitrarily large momentum, as nothing else depends on it. The kinematical variables of the photon are generated with the help of the distribution defined by the factor $\left[k_\gamma dk_\gamma d\cos\theta d\phi \frac{1}{2(2\pi)^3}\right]$; which provides the photon variables of the *tangent space*. Fully constructed with four-momenta, an event of the n-body decay can be turned back into a representation of angles and invariant masses. In the final step these angular variables, together with those of the photon, can be used to define a new event in the $(n+1)$-body phase space. In the case when the new kinematical variables do not fit the limits of available $(n+1)$-body phase space the new event should be rejected and the original configuration (in the n-body phase space) kept. An important property of the algorithm presented here is the full coverage of the $(n+1)$-body phase-space being assured. In this procedure, the difference between n-body and $n+1$ body phase-space Jacobians can be calculated in an unambiguous way and introduced in the same rejection step as for the phase-space limits[2].

The features and transformations of the phase-space parametrization presented here are at the heart of the construction of the PHOTOS kinematics and have been used since its beginning. To complete the generation of photons, the exact phase-space parametrization must be completed with a matrix element, with both virtual and real QED corrections included. Careful regularization of soft singularities must be performed[3].

independent), for the construction of the crude distribution of photon emission probability. Note that, in this space, the photons' four-momenta are unconstrained by energy–momentum conservation. The limits on the energies of the photons are arbitrary. We checked that, at the 10^{-4} precision level, the results obtained from our simulations do not depend on the particular choice. We leave the underlying formal aspect of the algorithm to future papers.

[2]The effects of matrix elements, including those of virtual corrections, have to be introduced at this stage as well. They are indispensable, for example, to calculate relative probabilities of configurations with distinct number of final-state particles.

[3]Volumes of the partial width attributed to the configurations with n, $n+1$ particles, etc., have to be normalized to the total width, both at the level of the tangent and the correct (final) phase space.

In the standard version of PHOTOS, as published in [1, 2], the expression

$$
\begin{aligned}
X_f^{\rm PHOTOS} = \quad & \frac{Q'^2\alpha(1-\Delta)}{4\pi^2 s}s^2 \quad \Bigg\{ \\
& \frac{1}{k'_+ + k'_-}\frac{1}{k'_-} \quad \left[(1+(1-x_k)^2)\frac{d\sigma_B}{d\Omega}\left(s, \frac{s(1-\cos\Theta_+)}{2}, \frac{s(1+\cos\Theta_+)}{2}\right)\right]\frac{(1+\beta\cos\Theta_\gamma)}{2} \\
+ & \frac{1}{k'_+ + k'_-}\frac{1}{k'_+} \quad \left[(1+(1-x_k)^2)\frac{d\sigma_B}{d\Omega}\left(s, \frac{s(1-\cos\Theta_-)}{2}, \frac{s(1+\cos\Theta_-)}{2}\right)\right]\frac{(1-\beta\cos\Theta_\gamma)}{2}\Bigg\} \\
& \text{where :} \quad \Theta_+ = \angle(p_+, q_+),\ \Theta_- = \angle(p_-, q_-), \\
& \qquad \Theta_\gamma = \angle(\gamma, \mu^-) \text{ is defined in } (\mu^+, \mu^-)\text{-pair rest frame,}
\end{aligned} \tag{4}
$$

is used for the real-photon matrix element. The virtual corrections are requested to be such that the total decay rate remains unchanged after complete QED corrections are included. The expression, without approximation, reads:

$$
\begin{aligned}
X_f = \frac{Q'^2\alpha(1-\Delta)}{4\pi^2 s}s^2 \quad & \Bigg\{ \frac{1}{(k'_+ + k'_-)}\frac{1}{k'_-}\left[\frac{d\sigma_B}{d\Omega}(s,t,u') + \frac{d\sigma_B}{d\Omega}(s,t',u)\right] \\
& + \frac{1}{(k'_+ + k'_-)}\frac{1}{k'_+}\left[\frac{d\sigma_B}{d\Omega}(s,t,u') + \frac{d\sigma_B}{d\Omega}(s,t',u)\right]\Bigg\}.
\end{aligned} \tag{5}
$$

The combined effect of the virtual and real corrections on the total rate is its increase by a factor of $1+\frac{3}{4}\frac{\alpha}{\pi}$.

The notation from ref. [21] are used:

$$
\begin{aligned}
s = 2p_+\cdot p_-, \quad & s' = 2q_+\cdot q_-, \\
t = 2p_+\cdot q_+, \quad & t' = 2p_+\cdot q_-, \\
u = 2p_+\cdot q_-, \quad & u' = 2_-\cdot q_+, \\
k'_\pm = q_\pm\cdot k, \quad & x_k = 2E_\gamma/\sqrt{s}.
\end{aligned} \tag{6}
$$

This paper collects complete first-order radiative corrections for the process $e^+e^- \to \mu^+\mu^-(\gamma)$. Final-state bremsstrahlung constitutes part of these results, where nonetheless reference is made to the incoming electron beam momenta.

The Δ term encapsulates final-state mass-dependent terms, p_+, p_-, q_+, q_-, k denote four-momenta of: incoming e^+, e^-, outcoming μ^+, μ^- and the bremsstrahlung photon respectively. Expression (5) is explicitly taken from ref. [21], on Monte Carlo MUSTRAAL, which is where the interested reader will find the details of the definitions of variables and expressions such as Δ, used in the formulae (4) and (5).

The ratio of (5) to (4) constitutes the basic element of upgrading PHOTOS functionality to the complete first order[4]. Nothing needs to be changed in the phase-space parametrization. The

[4]This is only true for PHOTOS being run at first order. For the multiple-photon radiation option, the iteration of the single-photon emission kernel (and thus also its weight) is performed; see section 5.

effects of the virtual corrections have to be included as well and have to be properly introduced in the normalization. The expression for the correcting weight could be chosen[5] simply as

$$wt = \frac{X_f}{X_f^{\rm PHOTOS}} \frac{1}{(1+\frac{3}{4}\frac{\alpha}{\pi})}. \tag{7}$$

For the purpose of constructing a Monte Carlo algorithm, however, it is more convenient to separate it into a sum of two generation branches (with slightly different angular variable mapping). Then, the expression for the distribution and those for the weight take the form

$$\begin{aligned}
X_f = &\quad X_f^1 + X_f^2 \\
X_f^1 = &\quad WT_1 \ \frac{Q'^2\alpha(1-\Delta)}{4\pi^2 s} s^2 \frac{1}{k'_+ + k'_-}\frac{1}{k'_-}\left[(1+(1-x_k)^2)\frac{d\sigma_B}{d\Omega}\left(s, \frac{s(1-\cos\Theta_+)}{2}, \frac{s(1+\cos\Theta_+)}{2}\right)\right]\frac{(1+\beta\cos\Theta_\gamma)}{2}, \\
X_f^2 = &\quad WT_2 \ \frac{Q'^2\alpha(1-\Delta)}{4\pi^2 s} s^2 \frac{1}{k'_+ + k'_-}\frac{1}{k'_+}\left[(1+(1-x_k)^2)\frac{d\sigma_B}{d\Omega}\left(s, \frac{s(1-\cos\Theta_-)}{2}, \frac{s(1+\cos\Theta_-)}{2}\right)\right]\frac{(1-\beta\cos\Theta_\gamma)}{2}, \\
WT_1 = &\quad \frac{\frac{d\sigma_B}{d\Omega}(s,t,u') + \frac{d\sigma_B}{d\Omega}(s,t',u)}{\left[(1+(1-x_k)^2)\frac{d\sigma_B}{d\Omega}\left(s, \frac{s(1-\cos\Theta_+)}{2}, \frac{s(1+\cos\Theta_+)}{2}\right)\right]\frac{(1+\beta\cos\Theta_\gamma)}{2}\left(1+\frac{3}{4}\frac{\alpha}{\pi}\right)}, \\
WT_2 = &\quad \frac{\frac{d\sigma_B}{d\Omega}(s,t,u') + \frac{d\sigma_B}{d\Omega}(s,t',u)}{\left[(1+(1-x_k)^2)\frac{d\sigma_B}{d\Omega}\left(s, \frac{s(1-\cos\Theta_-)}{2}, \frac{s(1+\cos\Theta_-)}{2}\right)\right]\frac{(1-\beta\cos\Theta_\gamma)}{2}\left(1+\frac{3}{4}\frac{\alpha}{\pi}\right)}.
\end{aligned} \tag{8}$$

At this point, let us make the following remark. Event though the introduction of the NLO weight into PHOTOS is trivial, the developed approximation [1] at the heart of PHOTOS design is not. It enabled universality of the program[6]. Simplification was not necessary to attribute the generation of bremsstrahlung photons to individual charged particles[7]. The separation holds for the complete NLO as well. The simplified emission kernel, which we used for other decays as well, reads:

$$\begin{aligned}
&\frac{Q'^2\alpha(1-\Delta)}{4\pi^2 s} s^2 \frac{1}{k'_+ + k'_-}\frac{1}{k'_-}(1+(1-x_k)^2)\frac{(1+\beta\cos\Theta_\gamma)}{2} \\
&\frac{Q'^2\alpha(1-\Delta)}{4\pi^2 s} s^2 \frac{1}{k'_+ + k'_-}\frac{1}{k'_+}(1+(1-x_k)^2)\frac{(1-\beta\cos\Theta_\gamma)}{2}.
\end{aligned} \tag{9}$$

[5] Alternatively, a factor $(1+\frac{3}{4}\frac{\alpha}{\pi})$ can be included in the definition of the crude distribution.

[6] Indeed, after inspection, the differences between formulae (4) and (5) are quite significant. The exact expression does not allow a transfer of the complete Born-level angular dependence to the host generator. In the correction weight, the two contributions, one depending on the angle Θ_+ and another on Θ_-, have to be simultaneously included. The dependence on the Born-level (effective) couplings thus need to be known at the level of the calculation of the final-state bremsstrahlung weight. This would make the modular structure of PHOTOS design more difficult to keep. Also, the direction of the (effective) beam need to be provided for the calculation of Θ_+ and Θ_- angles. This exhibits another difficulty in the separation of the final-state bremsstrahlung and the dynamics of the initial state for Z/γ^* production.

[7] For other decays, it will probably not be necessary to find an explicit form of such NLO separation. Starting from the NNLO, such separation was shown to be impossible [22] anyway.

It depends on the spin and charge of the "emitting particle" only[8]. It does not depend on the properties of the other decay products, which only define the phase-space limits. To obtain the universal form of the photon emission kernel, the interference was eliminated with the help of the factor, either $\frac{2}{(1+\beta\cos\Theta_\gamma)}$ or $\frac{2}{(1-\beta\cos\Theta_\gamma)}$. The interference is recovered later, using the weight given in formula (17) of ref. [2], that is with approximation. On the other hand, having paid the price of the approximated solution, both the kernel and the interference weight can then be used for decay of any particle or resonance.

In our present study the analytical expression for the matrix element for the $e^+e^- \to Z^0/\gamma^* \to \mu^+\mu^-$ is used (and compared to the approximated, yet process-independent, solution of the standard PHOTOS). If necessary, a matrix element for other decay processes (if available) could be used.

3. Method used in numerical tests

In the comparison of the multitude of final states generated, at different levels of physics sophistication by two distinct Monte Carlo programs, the choice of a method is of great importance. To compare the Monte Carlo programs it is quite common to present the distributions generated by the programs superimposed on a single plot, often in logarithmic scale. Such a method was used, for example, in ref. [23]. The method is unquestionably sufficient, if one's interest is limited to, say, the collinear content of the results or other distributions of the intrinsically logarithmic type.

For instance, applying this method for the comparison of the total energy carried out by all bremsstrahlung photons, we would obtain a distribution such as those presented in Fig. 1. We could conclude that there is excellent agreement, and the non-leading effects, which are essential for estimating systematic errors for generators like PHOTOS, would be marginalized in the presentation. This is also the case if for the same distribution (see right-hand side of Fig. 1) the method [13] based on MC-TESTER is used. The distributions are indeed dominated by the collinear content of the programs! For other distributions, sensitive to second-order matrix-element parts, missing in PHOTOS, the differences would become visible on the plots obtained normally from MC-TESTER. That is why, in the present paper, we will keep to that class of comparison plots. The comparisons are automated and standardized. This not only reduces the time needed for debugging the tests, but also allows for easy cross-comparisons of the results presented in our consecutive papers.

For a selected decay process, such as the Z/γ^* decay, the four-momenta of the decay products and their flavours are extracted from the event record in an automated way (thereby limiting the effort of setting up the appropriate analysis code and also the risk of accidental errors). The

[8] In the original PHOTOS documentation we called this well-controlled truncation of the kernel a "property (such) that leading-log (collinear) and infrared limits are properly reproduced". This explanation turned out to be misleading for many readers. One can get biased, and expect the collinear approximation not only for the kernel, but for the whole design of the algorithm. This would be a serious limitation of our program design if indeed, as suggested in ref. [23], "PHOTOS was based on collinear approximation". Fortunately it is not the case. Such confusion was not a concern for the users, until now: precision requirements were not as high.

Figure 1: *A typical plot for comparisons, as described in ref. [23]. We use it to illustrate our method. The histograms presented in the left and right plots have identical content, and show a comparison of KKMC [14] and PHOTOS used in Z decay. The total energy carried out by all final-state photons is presented. Red (darker grey) colour represents the results of KKMC, green (lighter grey) of PHOTOS with the NLO weight activated. Samples of* 10^7 *events were used in this comparison. The results are overwhelmed by the collinear/soft content of the predictions.*
If the W instead of Z decay was chosen, it would not be the case. There, NLO effects would be dominant for the part of the spectrum above $M_W/2$*. However, in that case, we would not profit from the second-order matrix element Monte Carlo, available for tests.*

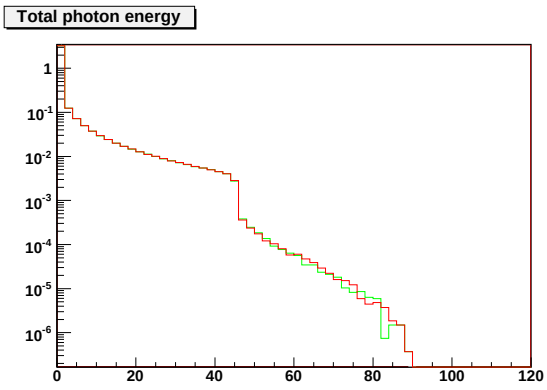

(a) A logarithmic scale is used. Excellent agreement between the two programs is visible all over the energy range from 0 to M_Z. The presence of the two lines can be spotted at the high end of the spectrum, mainly thanks to the statistical errors. The kink at the limit of the phase-space, where single hard-photon configuration ceases to contribute, dominates the content of the whole picture.

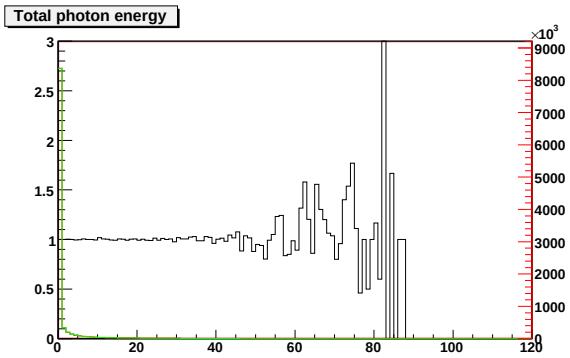

(b) *The method of MC-TESTER is applied. Both individual distributions, from PHOTOS and KKMC, are presented, but overlap. The samples populate the first few bins of the histograms. The differences would normally be visible on the black histogram, which presents the ratio of the results from PHOTOS and KKMC. The agreement is perfect all over the spectrum. No structure can be spotted in the vicinity of the kink (total photon energy, close to half of the Z mass). If present, the structure of possible differences, would be well separated from this of the shapes themselves.*

decay events obtained that way are classified in distinct decay channels, according to the particles present in the final state. The histograms of all possible invariant masses, which can be formed from the decay products, are defined and filled for each identified decay channel. At the end of the run they are stored in output files. Two output files (from distinct runs of event generators instrumented with MC-TESTER) are then analysed, and the results are presented in a form visualized as a "booklet" made of plots and summary tables. The user is given some general information concerning the comparison of the two runs with different Monte Carlo generators, a list of the decay channels with their branching fractions, and the maximum values (for each decay channel) of the shape difference parameter (SDP)[9].

For each decay channel the plots of histogrammed values are then included; each plot presents two distributions from the two distinctive runs and a curve, which is the ratio of the two normalized distributions. The value of the SDP is also printed for each plot. In practice, as in paper [13], the histograms obtained from the compared programs will often overlap. The differences will then be visible only in the plot of the ratio of histograms.

The testing approach implemented in MC-TESTER could be used directly in the case of validation of the TAUOLA package. Nevertheless, for the purpose of studies presented here, it needed an extension. It is necessary, according to the particular method of handling soft photon cancellations, to consistently treat the soft final-state QED bremsstrahlung photons, which may or may not be present in the event. If results of different programs were compared blindly, ambiguities due to differences in the treatment of the soft emission region and of the different boundaries for the photon phase-space (integrated analytically) would arise. To prevent these ambiguities, the most convenient solution was to introduce a technical regulator *in the test itself*.

For our comparisons to make physical sense and remain automatic, we had to remove the softest photons from the final states. We defined zero-, one-, and two-photon topologies in the following way: we called the event "zero photon" if there was no photon of energy (in a decaying particle's rest frame) larger than $E_{\rm test}$. The "one-photon" event had to have one (and only one) photon of energy larger than $E_{\rm test}$. If there were more than one such photons, we called it a "two-photon" event. In the case where there were more than two photons of energy larger than $E_{\rm test}$, we considered only the two most energetic ones, and treated the remaining (softer) ones as if they had not passed the $E_{\rm test}$ threshold. For all the photons that did not pass the $E_{\rm test}$ threshold we summed their four-momenta with the momentum of the outgoing fermion of smaller angular separation. With the help of our test we divide the phase space for two fermions and an arbitrary number of photons into *slots* of 0, 1 and 2 distinguished final-state photons.

In the paper we will use two variants of this test definition: *test1* and *test2*. The *test2* is exactly as explained above. In *test1*, only one photon (the most energetic one) will be accepted. The free parameter, $E_{\rm test}$ is chosen to be 1 GeV for all results presented in this paper.

Systematic histogramming of all possible invariant masses that can be constructed from a

[9]The shape difference parameter, defined in [24], quantifies the difference in shape of the histograms coming from the two runs being compared. The SDP value is calculated separately for each histogrammed mass: it quantifies the exclusive surface between the (normalized to unity) corresponding histograms obtained from the two runs. The effects of statistical fluctuations are appropriately subtracted. The maximum SDP over all distributions for a given decay channel is taken and printed in the table.

combination of final-state four-vectors, and storing them as one-dimensional histograms, does not define a test of ultimate sensitivity. The method is blind to the *P*-parity-sensitive effects, important for τ lepton physics, for instance. Also important effects, such as coherence between the photons are to a large degree washed out. Nonetheless we believe that the advantages of the method are prevailing, and we decided to use it in this study.

4. Results of the tests performed at first order

Let us start with a comparison of PHOTOS and KORALZ [25], both run at first order and without exponentiation. For KORALZ, the complete first-order matrix element, as in Section 2, is used. The results from KORALZ are given by a red (darker grey) line and from PHOTOS by a green (lighter grey) line. (In the presentation of the results we use the colour coding consistently in the plots and the summary tables, following the methodology of MC-TESTER). The lines overlap almost completely on all plots and only the ratios of the distributions shown as black histograms indicate that there is some difference. The actual plots for MC-TESTER comparison, are prepended with a summary table giving the fractions of event with and without photons (of energy above 1 GeV). In all comparisons samples of 10^8 events were used.

Decay channel	Branching ratio $\pm$ rough errors		Max. SDP
	KORALZ	PHOTOS	
$Z^0 \to \mu^-\mu^+$	$82.5137 \pm 0.0091\%$	$82.3622 \pm 0.0091\%$	0.00000
$Z^0 \to \mu^-\mu^+\gamma$	$17.4863 \pm 0.0042\%$	$17.6378 \pm 0.0042\%$	0.00534

As can be seen, the difference in the fraction of events with photon (of energy above 1 GeV) is about 0.15%. Although noticeable (thanks to our method), this is not a large discrepancy. Let us now turn to the distributions.

Decay Channel: $Z^0 \to \mu^-\mu^+\gamma$

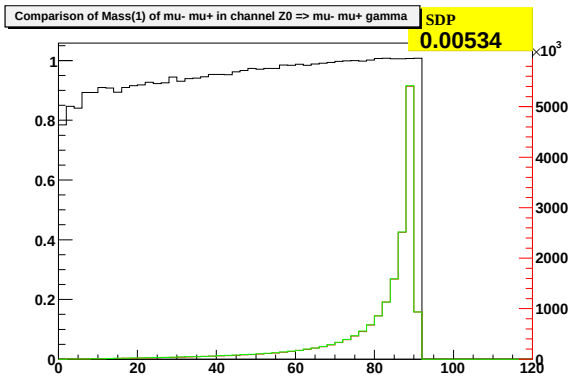

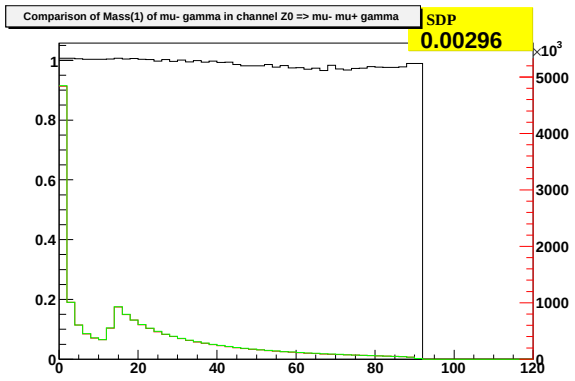

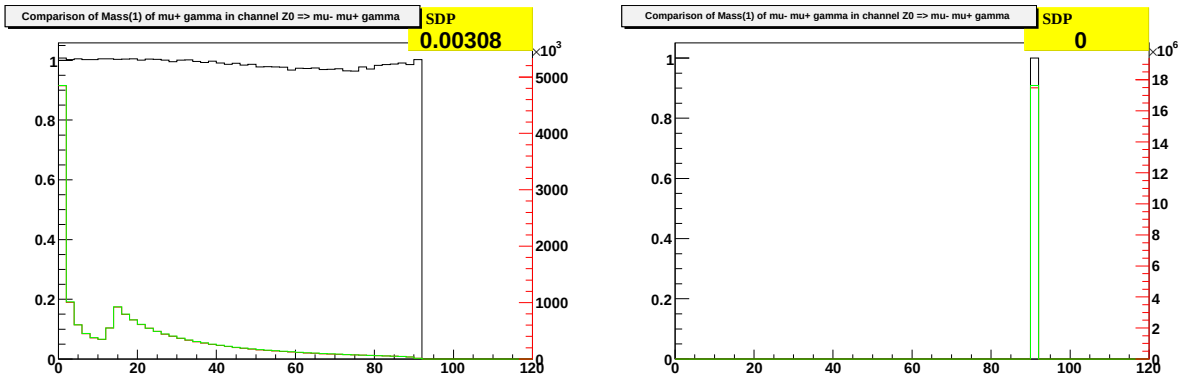

Analysing the values of the SDP, printed in the upper right corners of the plots, we conclude that the surfaces between green and red histograms (both normalized to unity before calculation of the ratio) differ by at most 0.005; this low value quantifies the fact that the histograms for the two programs overlap almost completely. The ratio of the two lines (black histogram) nonetheless reveals the difference, which is located at the far end of the spectra, sparsely populated by configurations with photons of extremely large energies and away from the direction of the muons.

Even though the agreement is amazing, it is yet improved once the NLO term is included into the correction weight of PHOTOS: the differences disappear below the statistical error of 10^8 event samples and they are not noticeable in the histograms' ratio curve either! In the following table and figures, we collect the results as previously discussed, but for the runs with the NLO correcting weight activated in PHOTOS.

Decay channel	Branching ratio $\pm$ rough errors		Max. SDP
	KORALZ	PHOTOS	
$Z^0 \to \mu^+\mu^-$	$82.5110 \pm 0.0091\%$	$82.5074 \pm 0.0091\%$	0.00000
$Z^0 \to \mu^+\mu^-\gamma$	$17.4890 \pm 0.0042\%$	$17.4926 \pm 0.0042\%$	0.00000

Decay Channel: $Z^0 \to \mu^+\mu^-\gamma$

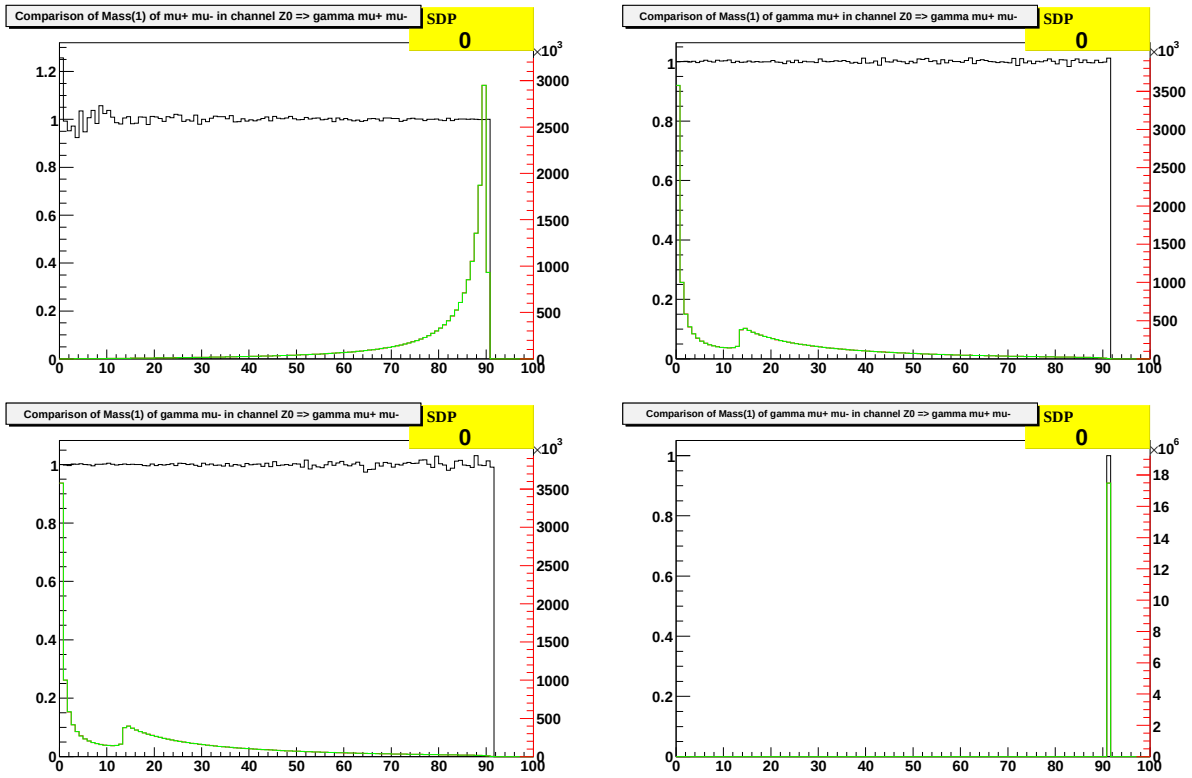

The agreement for the branching fractions (of events with and without photons of energy larger than 1 GeV) is better than 0.01% now! This excellent agreement indeed confirms that the theoretical effects missing in the standard version of PHOTOS are negligibly small. It is equally important that it provides, a powerful technical test of the generator. The kinematical variables used in PHOTOS differ from those of KORALZ; four-vectors are used instead of angles to parametrize the intermediate steps of the generation. The differences could have indicated, say, consequences of aggregation of rounding errors. Keeping in mind that similar levels of agreement for muons was achieved for the multiphoton version of PHOTOS and KKMC in the case of $Z \to e^+e^-$ decay, we can confidently claim that PHOTOS has numerical stability under control. This was not the case for the early versions of the program, and reaching that level of technical reliability required a major effort.

5. Algorithm for multiple-photon generation

Before presentation of the results for multiple-photon generation from PHOTOS, let us comment on those technical details of the PHOTOS algorithm, that are important in the implementation of the NLO contribution to the correcting weight. The iteration algorithm, as explained first in ref. [2], and recently also in refs. [12, 13], did not require changes for the case of multiple photon generation. Nevertheless, the following details have to be clarified for the proper implementation of the NLO weight, given by formula (8). All identical terms present in the

numerator and denominator, expressions (5) and (4) respectively, were cancelled out at the analytical level[10]. The weight (8) is always calculated for the single-photon configuration. If there are other photons generated in the previous steps of the iteration, their momenta are absorbed into the momenta of the final-state fermions. The constraint on the direction and the opening angle between the photon under consideration and the direction of the charged emitter [1], is assured.

6. Numerical results of the tests performed with multiple-photon radiation

Let us now turn to the tests of PHOTOS running in multiple-photon option. For that purpose we will use *test1* as defined in Section 3, and samples of 10^8 events generated from KKMC with exponentiation and the second-order matrix element and the multiple-photon radiation version of PHOTOS, without NLO terms. The results are included in the table and plots below.

Decay channel	Branching ratio ± rough errors		Max. SDP
	KKMC	PHOTOS	
$Z^0 \to \mu^-\mu^+$	$83.9176 \pm 0.0092\%$	$83.8372 \pm 0.0092\%$	0.00000
$Z^0 \to \mu^-\mu^+\gamma$	$16.0824 \pm 0.0040\%$	$16.1628 \pm 0.0040\%$	0.00409

Decay Channel: $Z^0 \to \mu^-\mu^+\gamma$

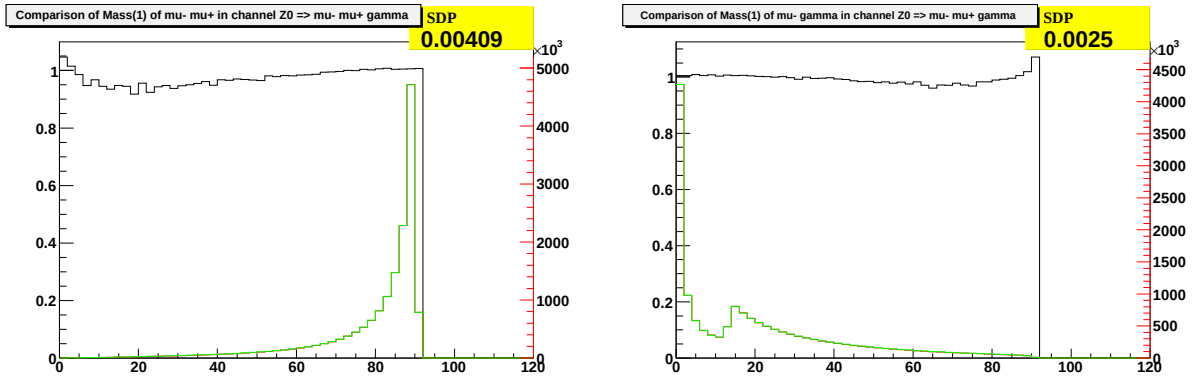

[10]The cancelled-out terms could have been calculated using slightly different kinematical variables; the differences would have appeared only in the case of more than one hard photon present in the final state. In such a case the ratio of the terms would not be equal to 1. These effects generally go beyond the NLO, and in fact our choice was motivated by the comparisons with the second-order matrix-element calculation, but without necessary details. That is why an appropriate discussion of this choice would require detailed presentation of the second-order matrix element. It would have to be similar, for example, to the discussion of the extrapolation procedure as that described in ref. [26].

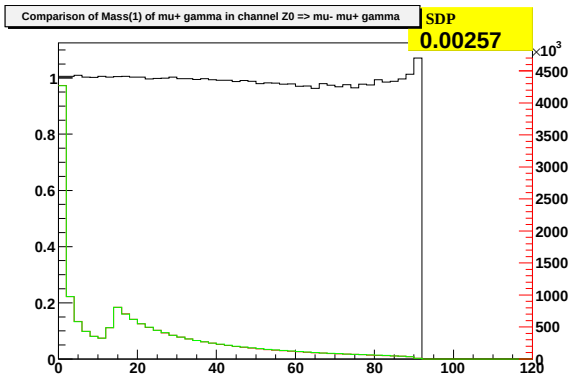

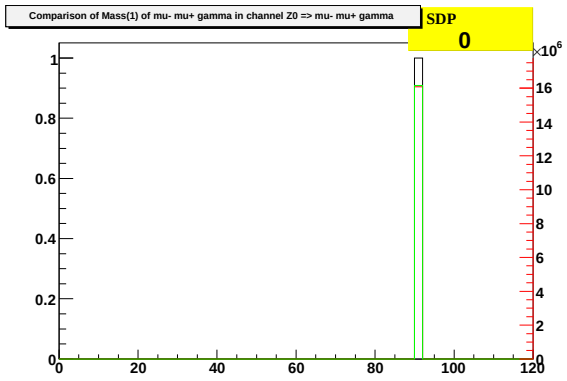

The pattern of differences between the results of PHOTOS and KKMC runs resembles the one present in the plots for the comparisons performed at the first order. Again, the black curves of the histogram ratios for the KKMC and PHOTOS results are not consistent with 1 for configurations with hard photons and in the regions where histograms are nearly at 0. The differences reach few per cent in the corners of the phase space contributing few per mille to the total rate. The discrepancies are again smaller than 0.1% with respect to the total rate.

Once the NLO weight in PHOTOS is activated, the already small differences become even smaller, by a factor of about 50, measured with the SDP. The differences are practically 0 with 10^8 samples, which can be seen in the table and the plots below.

Decay channel	Branching ratio $\pm$ rough errors		Max. SDP
	KKMC	PHOTOS	
$Z^0 \to \mu^-\mu^+$	$83.9176 \pm 0.0092\%$	$83.9312 \pm 0.0092\%$	0.00000
$Z^0 \to \mu^-\mu^+\gamma$	$16.0824 \pm 0.0040\%$	$16.0688 \pm 0.0040\%$	0.00003

Decay Channel: $Z^0 \to \mu^-\mu^+\gamma$

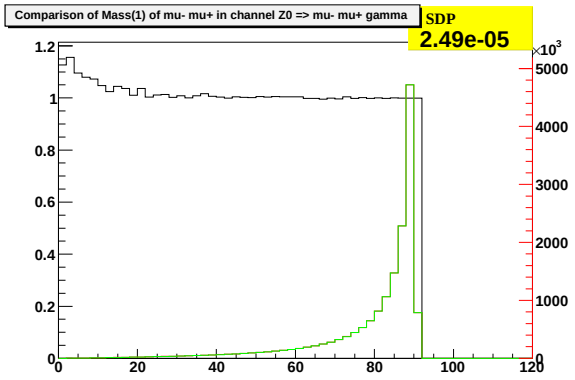

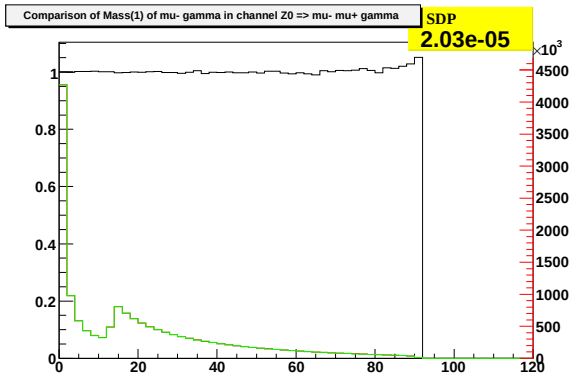

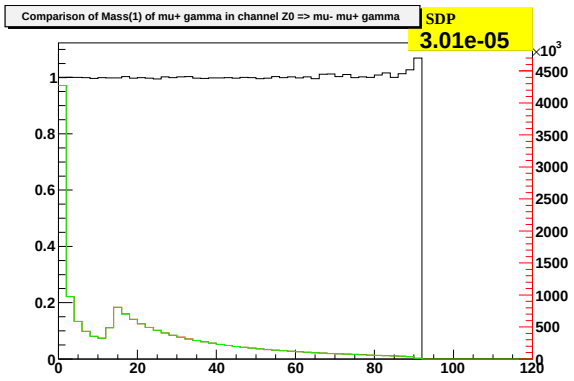

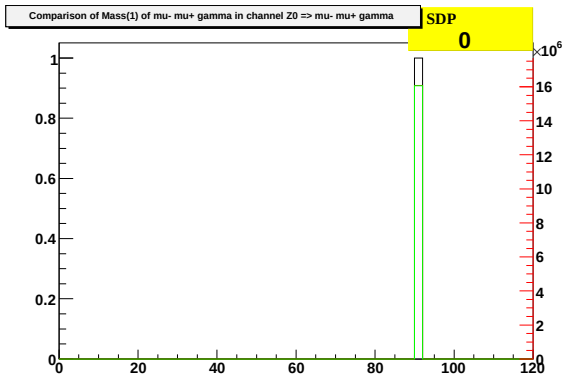

This confirms that the main source of residual discrepancy between KKMC and PHOTOS, both running in exponentiated versions, was due to the NLO term missing in the previous group of results and activated now.

Let us now turn to *test2*, where configurations of up to 2 hard photons are analysed. To this end, we will present at first the results of a comparison of the standard multiple-radiation version of PHOTOS with that of KKMC, followed by the comparison of multiple-radiation version PHOTOS with NLO weight and KKMC (again with second-order matrix element and exponentiation).

Decay channel	Branching ratio ± rough errors		Max. SDP
	KKMC	PHOTOS	
$Z^0 \to \mu^-\mu^+$	$83.9177 \pm 0.0092\%$	$83.8372 \pm 0.0092\%$	0.00000
$Z^0 \to \mu^-\mu^+\gamma$	$14.8164 \pm 0.0038\%$	$14.8676 \pm 0.0039\%$	0.00232
$Z^0 \to \mu^-\mu^+\gamma\gamma$	$1.2659 \pm 0.0011\%$	$1.2952 \pm 0.0011\%$	0.00918

Decay Channel: $Z^0 \to \mu^-\mu^+\gamma$

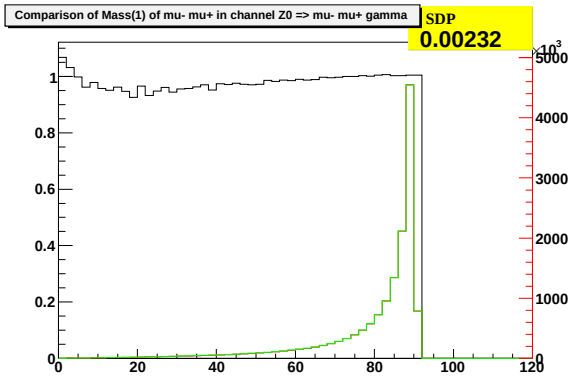

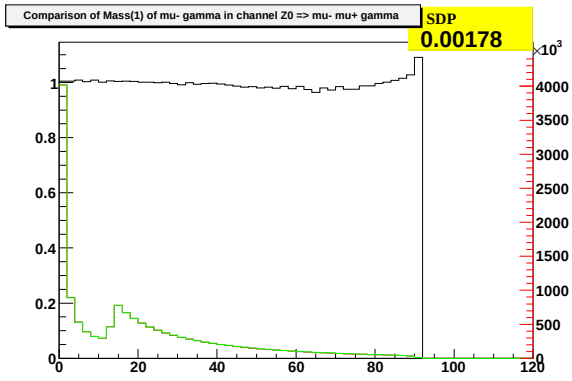

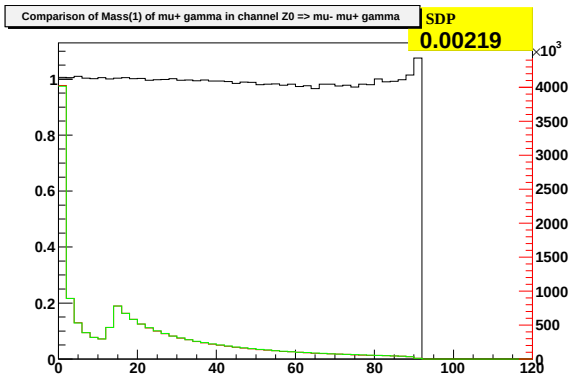

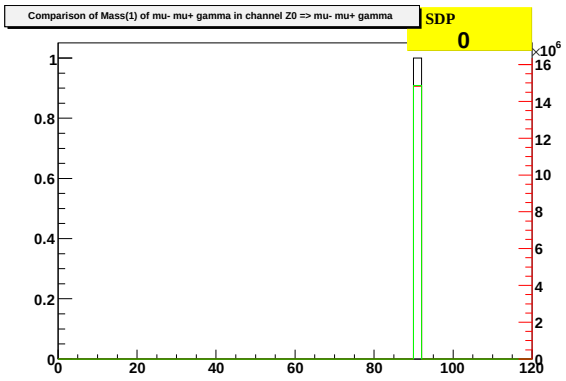

Decay Channel: $Z^0 \rightarrow \mu^- \mu^+ \gamma\gamma$

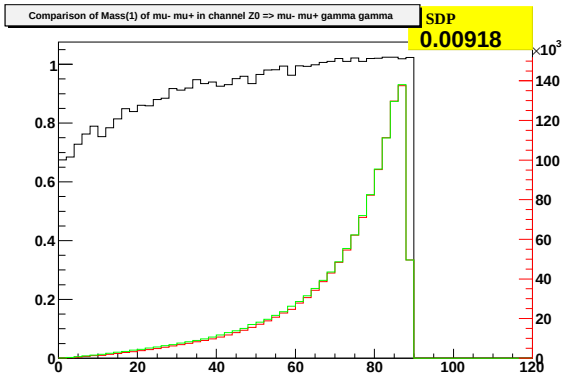

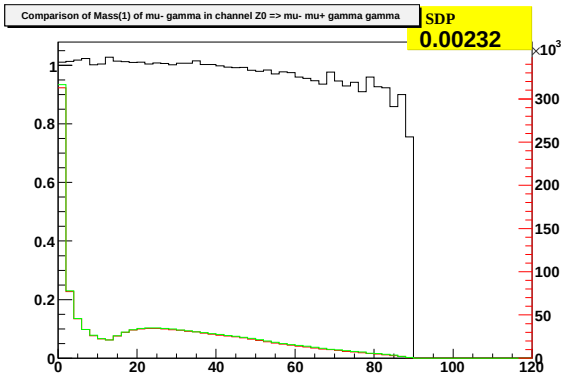

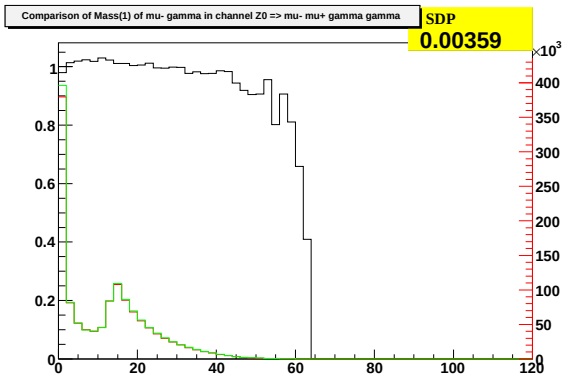

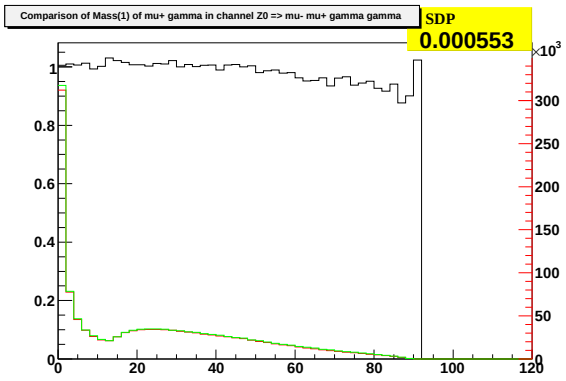

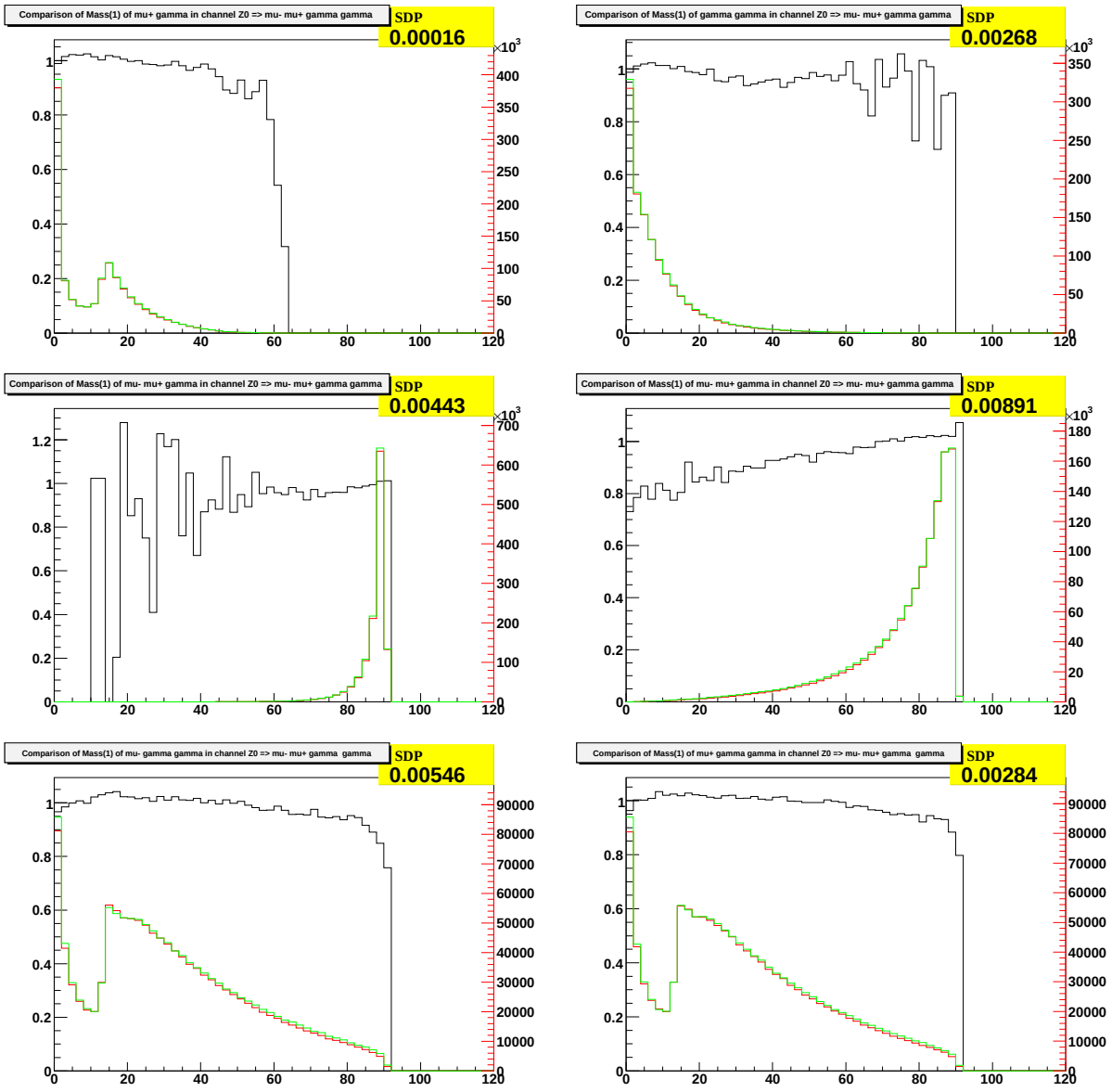

One can see that already for the standard PHOTOS the agreement is good. Residual deficiencies are small for both slots of the phase space: single hard photon, and two hard-photon. Let us present now what kind of changes the inclusion of NLO terms in PHOTOS brings to the results of *test2*.

Decay channel	Branching eatio $\pm$ rough errors		Max. SDP
	KKMC	PHOTOS	
$Z^0 \to \mu^-\mu^+$	$83.9177 \pm 0.0092\%$	$83.9303 \pm 0.0092\%$	0.00000
$Z^0 \to \mu^-\mu^+\gamma$	$14.8164 \pm 0.0038\%$	$14.7829 \pm 0.0038\%$	0.00005
$Z^0 \to \mu^-\mu^+\gamma\gamma$	$1.2659 \pm 0.0011\%$	$1.2868 \pm 0.0011\%$	0.00293

Decay Channel: $Z^0 \rightarrow \mu^- \mu^+ \gamma$

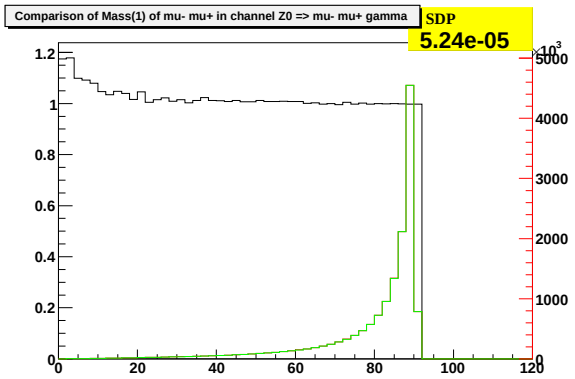

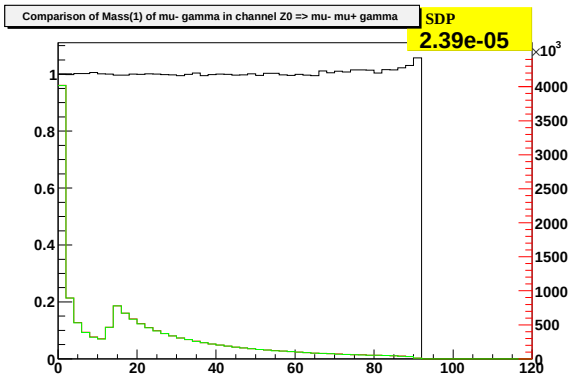

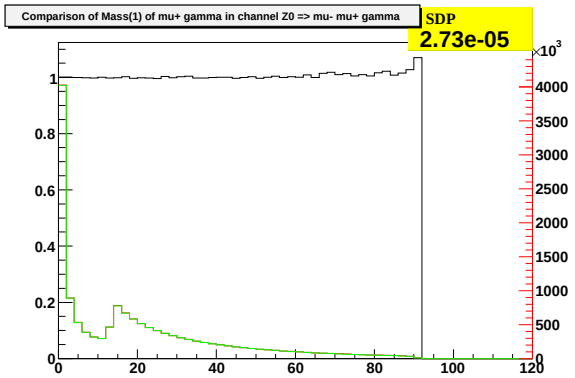

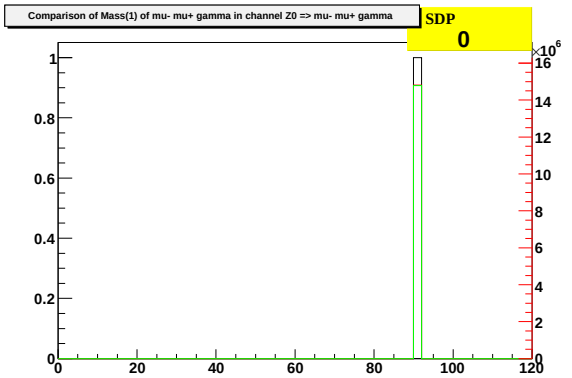

Decay Channel: $Z^0 \rightarrow \mu^- \mu^+ \gamma\gamma$

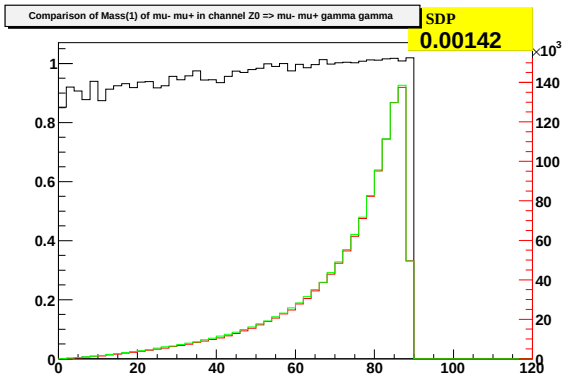

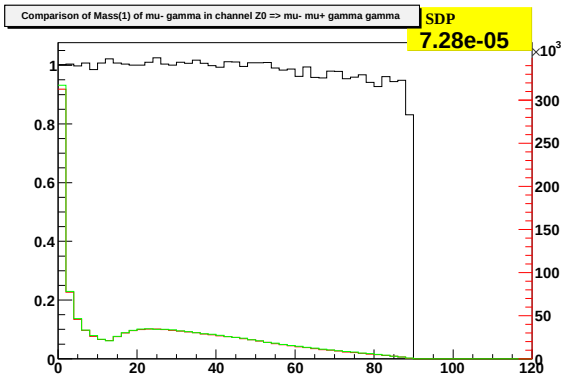

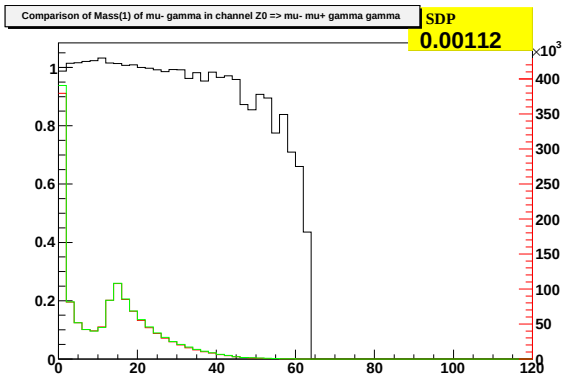
Comparison of Mass(1) of mu- gamma in channel Z0 => mu- mu+ gamma gamma
SDP
0.00112

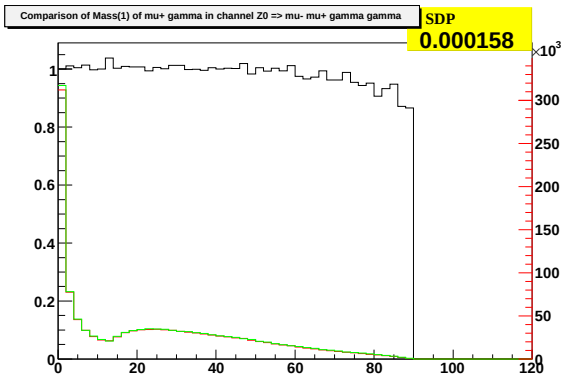
Comparison of Mass(1) of mu+ gamma in channel Z0 => mu- mu+ gamma gamma
SDP
0.000158

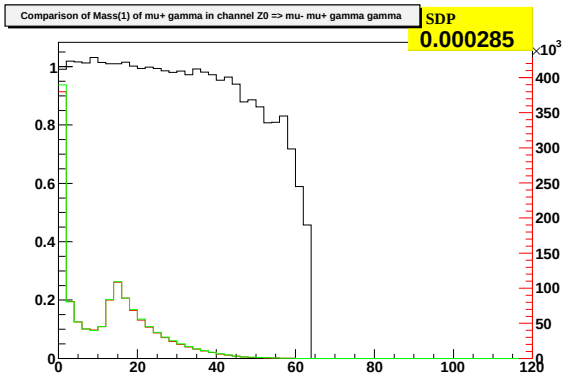
Comparison of Mass(1) of mu+ gamma in channel Z0 => mu- mu+ gamma gamma
SDP
0.000285

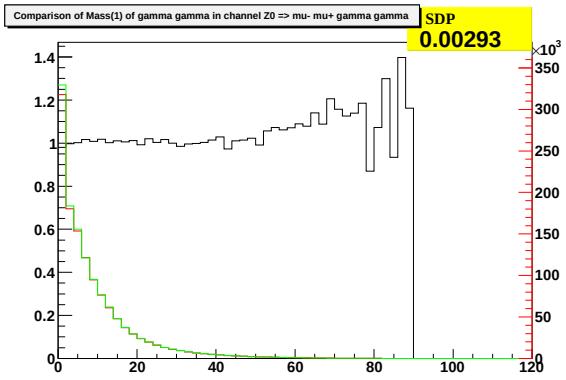
Comparison of Mass(1) of gamma gamma in channel Z0 => mu- mu+ gamma gamma
SDP
0.00293

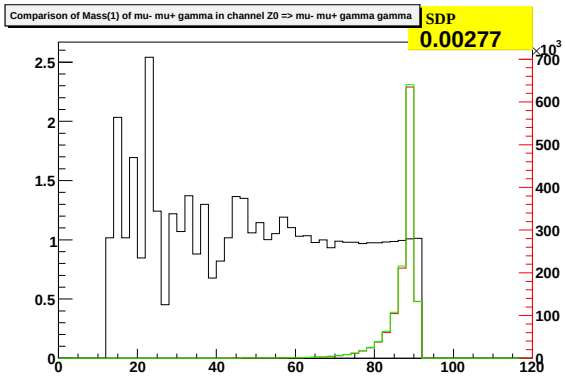
Comparison of Mass(1) of mu- mu+ gamma in channel Z0 => mu- mu+ gamma gamma
SDP
0.00277

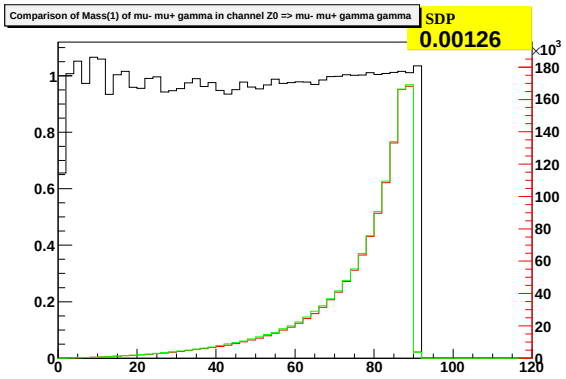
Comparison of Mass(1) of mu- mu+ gamma in channel Z0 => mu- mu+ gamma gamma
SDP
0.00126

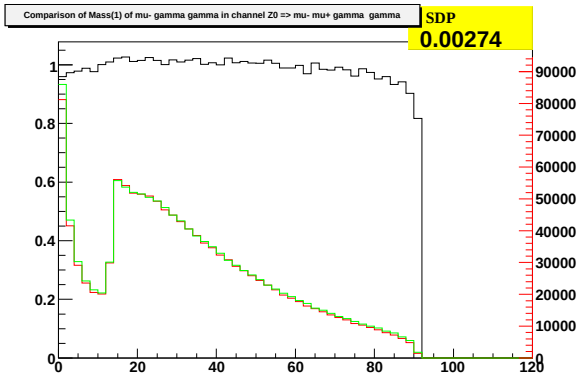
Comparison of Mass(1) of mu- gamma gamma in channel Z0 => mu- mu+ gamma gamma
SDP
0.00274

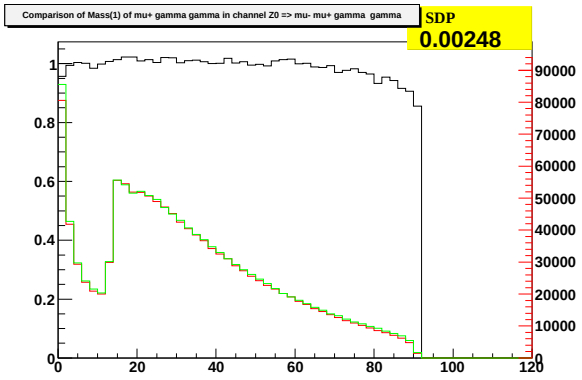
Comparison of Mass(1) of mu+ gamma gamma in channel Z0 => mu- mu+ gamma gamma
SDP
0.00248

For the single hard-photon distributions, the differences diminished significantly, again a factor of about 50! This was to be expected. Even for the distributions of the phase-space slot with two hard photons, the differences diminished. The SDP decreased by a factor of about 3. This is not as striking as for the single hard-photon configuration, but it is of no surprise: the complete second-order matrix element is missing. The improvement by a factor of 3 provides, however, a strong indication that the algorithm of iteration used in the generation of consecutive photons work well from the point of view of NNLL level as well. The acoplanarity plots presented in the previous paper [13] also demonstrated some of the NNLL aspect of the algorithm. That is why we are not going to discuss this point here, but we would rather leave it to future discussion of the NNLL content of our algorithm: this aspect goes beyond the purpose of the present paper and the scope of interest of most of PHOTOS users.

Much as is described in the present paper, a new contribution to the PHOTOS correcting weight would be needed for the NNLL case. However no changes in the phase-space algorithm would *a priori* be required. The techniques of gauge-invariant separation of the amplitudes into parts, as used for instance in ref. [26], will probably be necessary. They proved to be instrumental in the implementation of the second-order matrix elements for $e^+e^- \to \nu_e\bar{\nu}_e\gamma\gamma$ into KKMC. The exclusive exponentiation scheme of the KKMC Monte Carlo is prepared for *s*-channel processes.

We have to admit that once the NLO terms are switched on in PHOTOS, the difference between its results and those of the second-order matrix-element generator KKMC are at the limit of being recognized, even if samples of 10^8 events are used. For the case of the two-photon test, differences due to the missing second-order matrix element in PHOTOS can be observed; yet they are too small, and don't have enough structure, to understand their possible origin. A part of the differences may even originate from the third-order LL terms (after integration), which are missing in KKMC but generated in PHOTOS in the process of iteration.

In any case, even for PHOTOS running with standard options, the differences affect only a tiny fraction of the Z decay phase space. Thus, we do not consider it to be of much interest to continue the discussion of the missing terms. Nevertheless, from a more fundamental side, we are disappointed by the fact that the comparisons did not provide numerical insight into the structure of the differences. The particularly interesting aspects of the study in the context of the extension of the algorithm for QCD did not bring any constructive indications so far.

7. Summary

To quantify the size of the NLL effects, which are normally missing in PHOTOS, we reinstalled them back into the program, using the original complete first-order expression for Z decay. After the NLO correcting weight was installed, the differences between PHOTOS and KORALZ were below the statistical error of 10^8 events and for all the distributions used in the tests. Both PHOTOS and KORALZ were run at fixed first order without exponentiation. The agreement provided a technical cross-check test for the two simulations. For the case of multiple-photon radiation in PHOTOS, a comparison with the KKMC generator [14] (exponentiation and second-order matrix element used) was performed. The implementation of the NLO terms in PHOTOS indicated, in the results of our universal test, an improvement by a factor of

about 50 for the observables sensitive to a single hard photon in the final states and remained at the level of better than 0.1% on the total rate for all other cases we examined. Because of the smallness of the residual differences, it was difficult to understand their structure and origin in the final states with two hard photons.

The improvement in the agreement due to the introduction of the NLO correcting weight came at a price. Even though the weight is analytically simple and generation of weight 1 events remained possible, the calculation of the weight required information on Born-level coupling constants of the intermediate Z/γ^*. Also, the direction of the beam was necessary in the calculation of the weight. These requirements threatened the modular organization of the PHOTOS solution, as used in the large Monte Carlo generation chains of experimental collaborations. Numerically, the introduced improvements are rather small and the deficiencies of standard PHOTOS are localized in the corners of bremsstrahlung phase-space populated by photons of very high energies and angularily, well separated from the final-state muons. Those regions of the phase space weigh less than 0.005 to the total rate and the differences in that region approach 20% of their size. The effects are thus less than 0.1% of the total rate of the Z decay to muons. That is why we do not think it justified to complicate the PHOTOS algorithm and to enable the use of the NLO correcting weight in the general case.

The analysis presented here concentrates not only on the numerical results for the final-state bremsstrahlung in Z decay, but also on various aspects of a mathematical organization of the program for calculation of radiative corrections in Z production and decay. Separation of radiative corrections into parts: (i) embodied in effective couplings of the hard-scattering process, (ii) final-state QED bremsstrahlung, and (iii) initial-state bremsstrahlung, eventually with initial-state hadronic interactions, were mentioned as well. The effects of QED initial–final-state bremsstrahlung interference were to a large degree neglected. Such an approach is reasonable in the leading-pole approximation for the Z, but at a certain precision level the effects may need to be taken care of. For the time being the results of ref. [27] can be used instead.

Thanks to the analytic form of the kernel used in PHOTOS for the single-photon emission, the analysis presented here may easily be extended to other decay channels, if high precision is required and a calculation of matrix element is available. The study for the case of B meson decay into a pair of $\pi^{\pm}(K^{\pm})$ is near completion [28]. In this case the questions of reliability of scalar QED for the calculation of photons of high p_T, with respect to charged scalars, need to be addressed. A natural extension of the study of the systematic error in PHOTOS simulations, as presented here, would be the discussion of bremsstrahlung in W and Higgs boson decays.

The decays of the W and Higgs bosons are probably the only ones where formal studies of the NL terms, similar to the ones presented in this paper, can be performed. As was the case with Z decays, those cases will also be limited to the leading-pole approximation.

For other decay channels, the correction weight can be applied as well; however, in most cases the part of the weight going beyond soft and/or collinear regimes may need to be constructed with the help of the fits to the data. Let us stress that the unique design of PHOTOS, enabling the use of the same kernel for multiple-photon radiation (exponentiated) mode and at fixed first, second, third, and fourth orders, establishes a convenient environment for such fits of form factors to the data. At the same time the analytical form of these form factors can be taken from the first-order analytic calculations based on effective theory, or from any other model.

On the technical level it is worth mentioning that the NLO correcting weight of PHOTOS can be used as an internal correcting weight.

Finally, let us stress that the approximations introduced in PHOTOS affect the matrix elements and not the phase space. The generation of the latter is based on the tangent space constructed from eikonal approximation but used also for hard photons, even of energies above the available maximum enforced by energy–momentum conservation. Only in the second step are phase-space constraints enforced. This is similar to the case of the classical exclusive exponentiation. The energy momentum constraints are introduced for each individual photon, step by step, and conformal symmetry is not used in that procedure.

In principle, if necessary, complete higher-order matrix elements can be incorporated with the help of correcting weights. This point goes beyond the scope of the present paper. This is equally true for the possible extensions to simulations in QCD.

Acknowledgements. Useful discussions with Dmitri Bardin, Borut Kersevan, Maarten Bonekamp and Daniel Froidevaux are acknowledged. Special thanks go to Torbjörn Sjöstrand whose critical remarks convinced us of the necessity and urgency to perform the presented work.

References

[1] E. Barberio, B. van Eijk and Z. Was, *Comput. Phys. Commun.* **66** (1991) 115.

[2] E. Barberio and Z. Was, *Comput. Phys. Commun.* **79** (1994) 291–308.

[3] M. A. Dobbs *et al.*, hep-ph/0403045.

[4] CDF Collaboration, V. M. Abazov *et al.*, *Phys. Rev.* **D70** (2004) 092008, hep-ex/0311039.

[5] OPAL Collaboration, G. Abbiendi *et al.*, *Phys. Lett.* **B580** (2004) 17–36, hep-ex/0309013.

[6] DELPHI Collaboration, J. Abdallah *et al.*, *Eur. Phys. J.* **C31** (2003) 139–147, hep-ex/0311004.

[7] NA48 Collaboration, A. Lai *et al.*, *Phys. Lett.* **B602** (2004) 41–51, hep-ex/0410059.

[8] KTeV Collaboration, T. Alexopoulos *et al.*, *Phys. Rev.* **D71** (2005) 012001, hep-ex/0410070.

[9] Belle Collaboration, A. Limosani *et al.*, hep-ex/0504046.

[10] BABAR Collaboration, B. Aubert *et al.*, *Phys. Rev.* **D69** (2004) 111103, hep-ex/0403031.

[11] FOCUS Collaboration, J. M. Link *et al.*, hep-ex/0412034.

[12] P. Golonka and Z. Was, hep-ph/0508015.

[13] P. Golonka and Z. Was, *Eur. Phys. J.* **C45** (2006) 97–107, hep-ph/0506026.

[14] S. Jadach, Z. Wąs and B. F. L. Ward, *Comput. Phys. Commun.* **130** (2000) 260, Up to date source available from http://home.cern.ch/jadach/.

[15] S. Jadach, B. F. L. Ward and Z. Was, *Phys. Rev.* **D63** (2001) 113009, hep-ph/0006359.

[16] A. Nikiforov and Y. Ouvarov, *Éléments de la Théorie des Fonctions spéciales*, Editions Mir, Moscow, 1976.

[17] F. V. Tkachov, *Sov. J. Part. Nucl.* **25** (1994) 649, hep-ph/9701272.

[18] Z. Was, Written on the basis of lectures given at the 1993 European School of High Energy Physics, Zakopane, Poland, 12-25 Sep 1993, CERN-TH/7154-94.

[19] S. Jadach, Z. Was, R. Decker and J. H. Kühn, *Comput. Phys. Commun.* **76** (1993) 361–380.

[20] F. James, FOWL - a General Monte-Carlo Phase Space Program, 1977, CERN Computer Centre Program Library, Long Writeup W505.

[21] F. A. Berends, R. Kleiss and S. Jadach, *Nucl. Phys.* **B202** (1982) 63.

[22] R. Kleiss, *Nucl. Phys.* **B347** (1990) 67–85.

[23] K. Hamilton and P. Richardson, hep-ph/0603034.

[24] P. Golonka, T. Pierzchała, and Z. Was, *Comput. Phys. Commun.* **157** (2004) 39–62, hep-ph/0210252.

[25] S. Jadach, B. F. L. Ward and Z. Was, *Comput. Phys. Commun.* **66** (1991) 276–292.

[26] Z. Was, hep-ph/0406045.

[27] S. Jadach and Z. Was, *Phys. Lett.* **B219** (1989) 103.

[28] G. Nanava and Z. Was, In preparation. See transparencies: http://piters.home.cern.ch/piters/MC/PHOTOS-MCTESTER/AtNLO/Plot_B_PiPiGamma.pdf.